ASME Journal of Engineering for Gas Turbines and Power
Online journal at:
https://asmedigitalcollection.asme.org/gasturbinespower

Optimized H-Shaped VAWT for Tilted Operation: Computational Fluid Dynamics Evaluation of Design and Off-Design Conditions

Otman Kouaissah
Department of Engineering and Applied Sciences,
University of Bergamo,
Viale Marconi, 5,
Dalmine (BG) 24044, Italy

Nicoletta Franchina[1]
Department of Engineering and Applied Sciences,
University of Bergamo,
Viale Marconi, 5,
Dalmine (BG) 24044, Italy
e-mail: nicoletta.franchina@unibg.it

Giacomo Persico
Laboratory of Fluid Machines,
Department of Energy,
Politecnico di Milano,
Via Lambruschini 4,
Milano 20156, Italy

Muhammad S. Siddiqui
Faculty of Science and Technology,
Norwegian University of Life Sciences,
Drøbakveien 31,
Ås 1433, Norway

In the present work, a numerical investigation on the performance of an optimized H-shaped vertical-axis wind turbine (VAWT), previously presented at the ASME Turbo Expo, is provided both at design and high load condition, with the wind rotor operating at 20 deg of tilted angle (the static tilt angle of VAWTs commonly ranges between 10 deg and 20 deg). Unsteady computational fluid dynamics simulations have been adopted to explore the aerodynamics and near-wake characteristics of the selected machine, designed for operation in tilted conditions, typical of spar-buoy platforms. Combined effect of blade coning angle and flow skew angle is discussed with respect to the local performance to shed light on the effectiveness of energy harvesting pertaining to different machine portions. The analysis has been conducted over a large-scale model to estimate the wind rotor performance under possible, more feasible, conditions. The findings contribute with valuable insights for the ongoing development of floating-VAWT technology. Offshore wind power is increasingly recognized as a pivotal solution for renewable energy, with wind turbines located far from the coast offering unique advantages. The presented results offer detailed analysis of aerodynamic loads and performance over extended periods, showing good potential for innovative designs. [DOI: 10.1115/1.4069617]

Keywords: computational fluid dynamics, tilted VAWT, near wake, design and off-design VAWT

1 Introduction

Renewed interest in the technical development of vertical-axis wind turbines (VAWTs) is raised in the last few years, driven by the need of innovative solutions to pursue a green energy transition. VAWTs are characterized by a simple design, lower maintenance, and installation costs than horizontal-axis wind turbines since the generator is placed at the bottom of the machine and no yawing and tracking systems are required. Furthermore, high-density clustering can be considered in wind farm design in virtue of faster wake recovery, as shown, e.g., in Refs. [1–3]. Studies have also faced the issue of the Reynolds number effect, showing the higher potential of VAWTs scalability [4–6]. A review of possible VAWTs installations in offshore context has been suggested by investigations already presented in the open literature [7]. However, the inherent complex aerodynamics of these machines still require understanding and investigation to fully comprehend the vortical structures evolution within the rotor and behind it. Challenges are still posed and hinder the actual deployment of this kind of turbines [8]. For example, issues related to the reliability of the turbine arise because of the fatigue caused by the fluctuating loads occurring during typical operations. Cyclic torque variation during the rotor revolution may determine critical operating conditions [9].

Two different rotor designs were considered, studied, and modified during years, i.e., H-shaped and Troposkein-shaped. The former features ease of manufacturing, with two to five blades and a number of connecting struts. The latter one is obtained using two or more bent blades attached to the shaft at their top and bottom parts. To foster their adoption in offshore wind farms, further efforts must be carried on, to broaden the field of knowledge and promote dedicated design. The actual deployment of VAWTs in offshore applications requires advanced solutions in the trend of larger rotors to reduce the LCOE, thanks to their promising capability of scale-up with lesser technical concerns [10]. Aerodynamic fatigue and structural concerns must be faced to reach a new generation of wind turbines deployed in wind farms. VAWT competitiveness can be fostered by securing their advantages in terms of favorable rotor scaling, easiness of installation and maintenance, and reduced levelized cost of energy. Several studies have investigated through measurements or numerics the performance sensitivity with respect to relevant design parameters, such as the blade shape, airfoil design,

Turbo Expo: Turbomachinery Technical Conference & Exposition (GT2025), June 16–20, 2025. GT2025.
[1]Corresponding author.
Manuscript received July 23, 2025; final manuscript received August 1, 2025; published online October 31, 2025. Editor: Jerzy T. Sawicki.

solidity, and rotor aspect ratio, to name a few, in order to shed light on issues that characterize the performance of a VAWT [11–14]. As indicated in Ref. [15], the H-shaped and the Y-shaped rotors offer good potential cost-effective offshore designs. A technical advantage of H-rotors is the adoption of the connecting bar as an aerodynamic brake system without expensive modification of the blades.

A design featuring a different coning angle in the upper and lower parts of the turbine was considered in the X-rotor concept [16], where blades were conceived as angled up and down elements with coning angles of 30 deg and 50 deg, respectively. Such a design has been fully assessed both in aerodynamic and structural terms [16,17]. To enlarge the fields of knowledge and dataset available for H-based designs, the current investigation considers the modified H-shaped geometry to discuss its the performance and near-wake establishment.

In the present work, further development with respect to the performance analysis of an optimized H-shaped rotor is presented to broaden the results provided in Ref. [6] where two modified H-shaped designs were introduced and investigated. The wind rotor is composed of three blades with a coning angle and operates in a tilted position. Critical evaluation of the flow field at varying operating conditions is complemented with detailed description of the local torque at shaft, collected by specific region of the blades, selected in spanwise manner. The two parts of the rotor, defined by the holding strut, display different peculiar behavior. The detachment of vortices in the downstream is reported and related to the near wake shape and development.

2 Case of Study

The wind turbine considered in the current study has been presented in Ref. [6] and therein named HV2. This wind rotor was considered along with another model, named HV1, conceived with a different blade coning angle design. These two machines were evaluated in terms of energy harvesting capability and near-wake development against a standard H-shaped one. The performance prediction of the HV2-shaped rotor indicated a power harvesting capability enhancement up to 30% with respect to the standard straight blades H-design. Good near wake mitigation was observed in the near wake for both the HV-shaped designs. However, the better balance in between power harvesting and wake mitigation was found for the HV2 model, as reported in Ref. [6]. Therefore, in the current work, this solution optimized in terms of overall performance is further considered to broaden the knowledge of complex flow field developing at relevant tip speed ratio (TSR) values, i.e., a near peak power and high-load conditions.

A brief description of the main characteristics of the HV2 rotor is provided. It is a modified H-shaped, three-bladed, VAWT endowed of a single aerodynamic holding strut. Each blade is defined using a NACA0021 profile that is swept along the span with coning angle equal to 10 deg. Figure 1 displays the wind turbine lateral view along with the reference coordinate system and the definition of relevant regions used to describe the energy harvesting of the machine. Spanwise slices can be observed (10 equally spaced and 14 in the lower and upper regions, respectively) defined in an orthogonal way with reference to the rotation axis. The figure displays a typical detachment of vortices due to blades and flow interaction, giving the first indication of complex structures occurring during the machine revolution. Their understanding can better be obtained if local flow features are carefully analyzed.

Table 1 summarizes the main geometric parameters of the rotor, corresponding to a large-scale machine (some of which are also visible in Fig. 1).

The operating conditions are selected according to typical average wind speed values. The skew static angle was chosen equal to $\beta = 20$ deg, according to previous studies on the effect of flow skewness on the performance of wind turbines [14,18–20]. Following indications on typical TSRs interest, two values have been considered, namely, a possible design point identified at

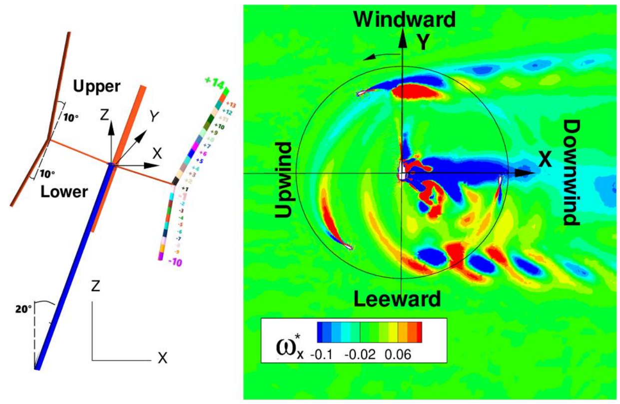

Fig. 1 H-shaped VAWT: geometry, spanwise slices, upper and lower rotor region, cross section regions of interest

Table 1 VAWT geometrical parameters

	(m)
Lower blade part	60.6
Upper blade part	84.6
Chord	6.06
Rotor radius at strut	60.6
Solidity	0.3

TSR $= 2.9$ corresponding to 11 m/s of approaching freestream wind, and a high-load, lower velocity case with TSR $= 4.55$, i.e., 7 m/s. The selected rotor is a full-scale model, its dimension pertains to a power generation of some MegaWatts. The regime characterizing the machine is fully turbulent, as the reference Reynolds number is of order 10^6. The turbine is considered by varying the freestream wind velocity and keeping fixed the revolution per minute, equal to five revolutions per minute.

3 Numerical Methodology

A three-dimensional (3D) unsteady incompressible flow model is considered to fully account for vortical structure evolution and their interaction with solid walls. A reliable and accurate approximation of the flow field in terms of global and local performance can be obtained by considering the unsteady Reynolds-averaged Navier–Stokes equations as already reported in several investigations presented in the literature [14,21,22] Following the guidelines presented in Refs. [20] and [23], second-order accurate schemes in space and time are applied to the unsteady Reynolds-averaged Navier–Stokes governing equations equipped with the $k - \omega$ shear stress transport two-equation turbulence model by Menter [24]. This model is well-established and widespread in the turbomachinery field and demonstrated to be a good tradeoff between accuracy and computational cost.

The discrete equations are solved using a pressure-based algorithm of coupled type, and an algebraic multigrid solver is adopted to solve the final discrete system up to an accuracy level of 10^{-5} evaluated using the norm of scaled residuals. The discrete domain must be properly defined in order to avoid spurious oscillations, artificial blockage effects, or numerical artifacts. However, it must also be minimized to avoid a prohibitive computational cost. The adopted 3D domain is defined by an inlet boundary placed 4.5 diameters upstream of the shaft, an outlet surface at 3D downstream, and the lateral ones at 3D apart from the shaft itself (following Refs. [20] and [23]). The computational domain is subdivided into nonoverlapping elements (20×10^6 of polyhedral cells) defined through dedicated sensitivity analysis. To fulfill accuracy requirements, the first cell height off the solid wall

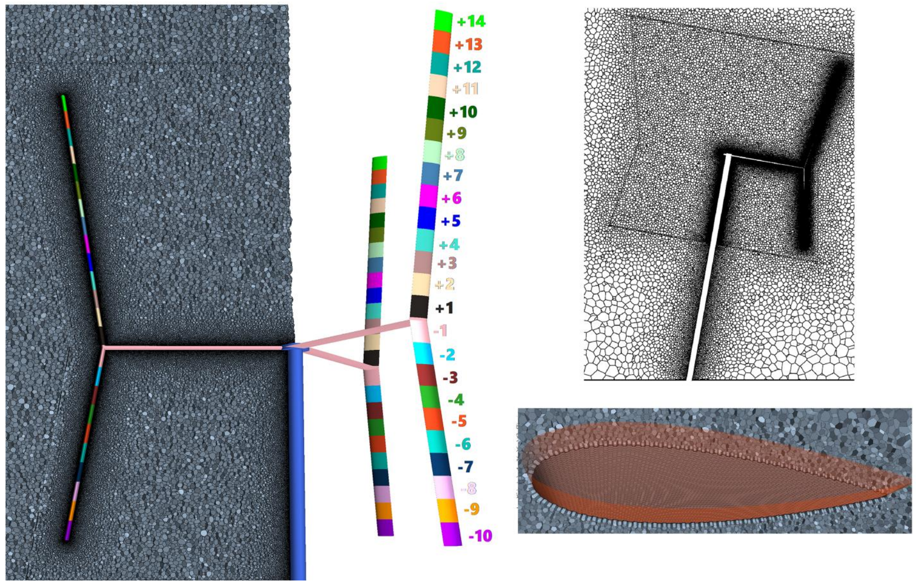

Fig. 2 Computational grid: near wall zoom near airfoils and strut, at symmetry plane *XY* and near the shaft at *Y*=0 plane

was defined in order to match the $y^+ \approx 1$. Overall view and details near solid walls of the mesh are shown in Fig. 2. The boundary conditions used are reported in the following: (i) at the inlet region, the freestream velocity, a turbulence intensity of 1a turbulent viscosity ratio equal to 1 were prescribed, (ii) at lateral, downstream, and top boundaries, the static pressure was imposed, and (iii) instead, the no-slip condition was selected at solid shaft and blades surfaces and on the ground.

The computational time-step corresponding to 720 discrete steps per revolution has been selected starting from results already presented in the literature by the authors. Afterward, the validity of this value has been checked through a dedicated sensitivity procedure relying upon convergence criteria set on the C_P value. This quantity, evaluated in between subsequent revolutions, was considered satisfactory below 2% relative error. Simulations have been carried out for the selected TSR values till periodic solution achievement. The periodicity of the solution was achieved after about 20 revolutions.

Computations have been performed using the multiphysics solver STAR-CCM+ by Siemens, Siemens Digital Industries Software (Italy). The simulations were carried out on the high-performance computing cluster provided by the Norwegian Research Infrastructure Services (Sigma2). Each case required approximately two weeks of computational time, relying upon 64 processors.

Finally, notice that in this work, dedicated validation is not available, being the wind rotor a possible design of large-scale multi-MW machine. However, the whole numerical setup employed has been extensively validated against experimental results for a similar lab model [25], see the Appendix showing the satisfactory agreement of predictions against measurements.

4 Vertical-Axis Wind Turbine Performance and Flow Physics

The complex unsteady flow field developing within a VAWT directly determines the performance of the machine and the understanding of relevant physical issues can be described using both global and local evaluations. Wind turbine performance is typically reported with the power coefficient as a function of the operating condition expressed by the TSR value, giving rise to the characteristic curve. Power generation is then expressed in terms of generated MW. For the HV2 large model herein investigated, at peak power condition (TSR = 2.9) and at high load, off-design, operation (TSR = 4.55), the performance data are reported in Table 2. These global data give an indication on the machine capability, but they demand for detailed investigation of local flow issues to understand how these data are obtained.

Table 2 HV2 wind rotor: power coefficient and generated power as a function of TSR value

TSR	C_P	P (MW)
2.9	0.34	6.14
4.55	0.24	1.22

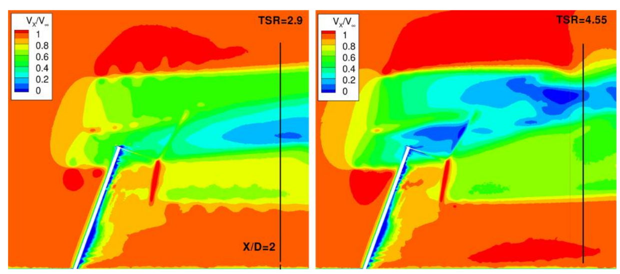

Fig. 3 HV2 wind rotor: streamwise velocity at *Y*/*D*=0 at two TSRs

First evaluation of the different flow field giving rise to these values is provided in Fig. 3 which displays the nondimensional streamwise velocity at $Y/D = 0$ section for both TSRs. These flow contours suggest the following observations: At high load: (i) higher viscous effects are predicted; (ii) major blockage determines a larger velocity defect in the wake. At peak power: (i) enhanced aerodynamic efficiency is expected along with a major tendency at stall occurrence.

The actual flow structures are fully 3D, and the streamwise velocity allows to obtain indications of the harvesting capability. The spanwise evolution of velocity can be observed, for example, to discuss suction effects that do modify the wake extent and recovery. In fact, the flow-spanwise history needs to be carefully estimated to better describe the wake establishment. In Fig. 4, the $Z-$ component of the velocity is displayed at $Y/R = 0$ cross section. In the leeward region of the revolution, where the flow structures already encounter the rotating blades, vertical flow paths are observed. Upward

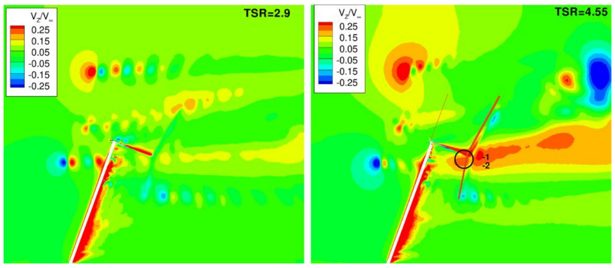

Fig. 4 HV2 wind rotor: spanwise velocity at $Y/D=0$ at two TSRs

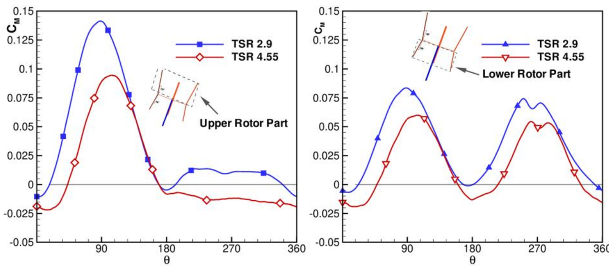

Fig. 5 Torque coefficient at TSR 2.9 and 4.55: torque pertaining to the upper and lower parts of the rotor

movement of the flow is displayed at a larger extent for the high TSR value, especially from slices −1 and −2 (just below the connecting strut). Larger-scale vortices are promoted, and faster recovery may occur.

Figure 5 displays the moment coefficient computed for the upper and lower parts of the rotor, namely, above and below the holding strut. Considering the rotor tilt, the upper part of the machine is operating like a common H-shaped turbine with most of the energy extraction coming from the upwind part of the revolution. The remaining amount of energy poorly contributes to the harvesting task or even stems into a braking effect, as in the case of TSR = 4.55. The maximum torque coefficient is reduced by 35% passing from the peak to the high load conditions.

Instead, the lower part of the machine (featuring a reduction of about 27% from TSR 2.9 to 4.55) displays a different behavior. In fact, in this region, the effective blade inclination varies depending on the position. Specifically, in the upwind position, the effective inclination is 30 deg, derived from the sum of the 10 deg coning angle and the 20 deg tilt angle. Conversely, in the downwind position, the effective inclination is reduced to 10 deg, calculated by subtracting the 10 deg coning angle from the 20 deg tilt angle. So the reduced C_M in the upwind is balanced with an increased one in the downwind, and the blades traveling in the upwind are characterized by lower effective incoming velocity, giving rise to lower maximum torque (minus 20%). However, when the blades are operating in the downwind region, they can exploit the boost effect due to fresh air and thus a more advantageous aerodynamics. The torque coefficient of the lower rotor part, in the downwind region, achieves a 60% increase in C_M concerning the same region considered for the upper part of the rotor. Considering the nearly equal torque highlighted in upwind and downwind, the lower rotor part is contributing with a more regular overall torque acting on the shaft.

The performance of the lower half part of the machine is influenced by the design and operating conditions. The upwind region can benefit from more effective incoming velocity, particularly in the leeward zone in the upwind. Furthermore, a nearly perfect balancing of torque at downwind with that pertaining to the upwind is obtained, as shown in Fig. 6 where the C_M is displayed at the tip slice −10 and medium slice at −5. For both TSR values, the upwind and downwind regions show profiles that are similar to one another. Better aerodynamic behavior is obtained at TSR = 2.9 with a higher maximum C_M, earlier achieved than at

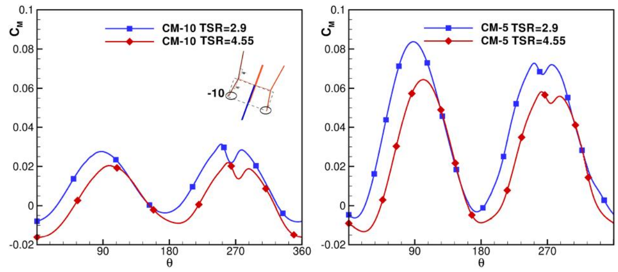

Fig. 6 Local torque coefficient at peak power and high-load: lower part of the rotor, slices −10 and −5

TSR = 4.55. The anticipated stall is however followed by the same decrease in torque. Comparison of the C_M profiles pertaining to the slice −10 with −5 allows to appreciate the torque reduction due to the finite blade effects. Rotor parts corresponding to the middle region of blades, such as −5, register a higher torque coefficient.

Furthermore, in the lower part of the VAWT, vertical flow movements promoting a wake enlargement as shown in Fig. 7 can be observed. While moving from bottom toward the strut at $Z^* = 0$, a suction effect upward is noticed both in the windward and leeward sides of the downwind. This action is tightly connected to the operated, low velocity, tilted condition.

Near the connecting strut, the performance at high load is somewhat limited because of viscous effects playing a role. Negative, braking, torque is observed in this region, see Fig. 8 with comparison against a higher freestream velocity, namely, at TSR = 2.9.

The upper part of the machine is characterized by a well-known torque profile trend, in which the largest quota of energy is obtained in the upwind, and very low or null contribution is provided instead by the blades traveling in the downwind. Good performance can be appreciated in a region far away from the strut and tip blade, such as the slice +7. Significant reduction of the available torque near the tip (slice +14) due to the finite length effects is instead clearly visible; see Fig. 9.

Finally, the local power computed from the bottom to the top of the machine is reported in Fig. 10 where the MWs locally produced are referred to the local reference section. Spanwise slices, labeled with negative and positive integers, are those given in Fig. 1. This local power evaluation provides a graphical representation of the machine's effectiveness and local losses. Finite blade effects are reported as a function of the load occurring and viscous losses connected to the presence of the holding strut, also scaling with the relevance of viscous losses. The figure quantifies the good performance at peak power, for an estimated total power of 6.14 MW against 1.22 MW at high load. Similar trends are found for the considered TSR cases, even though clearly more uniform harvesting is observed in the high load case.

5 Near Wake Evolution

The actual capability of energy harvesting directly impacts the wake shape and evolution, and its morphology can be tightly connected to the rotor blade design and operating conditions [19,26–29]. In this section, the near-wake development is described through local and global flow features evolution. In Fig. 11, the near wake contours are depicted at a streamwise cross section $X/D = 2.0$ and complemented by the transversal wake profiles at three stations Z^*, also reported in the figure for the sake of clarity, labeled A, B, C from bottom to top (−R, 0, R). The same velocity map and profiles are reported for TSR = 4.55 in Fig. 12. At first glance, the high load condition, being affected by a greater blockage, is characterized by larger and deeper velocity defects. A major drag contribution is imparted at TSR = 4.55, and a nonsymmetric wake can be observed in the lower part of the machine (see vertical movements already commented in Fig. 7), for example, at Z^*_A, with a larger defect velocity in the leeward region of the revolution. While moving upward, the wake becomes nearly symmetric, larger, and deeper.

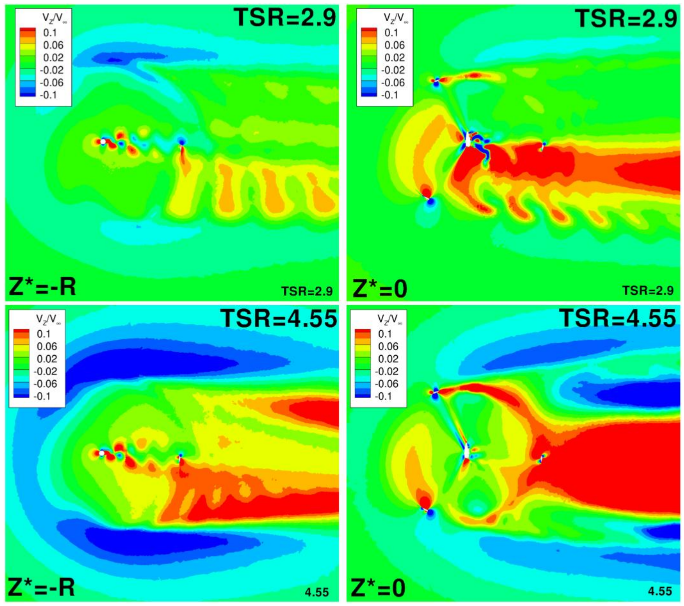

Fig. 7 Spanwise velocity at TSR 2.9 and 4.55 for two selected span positions Z^*

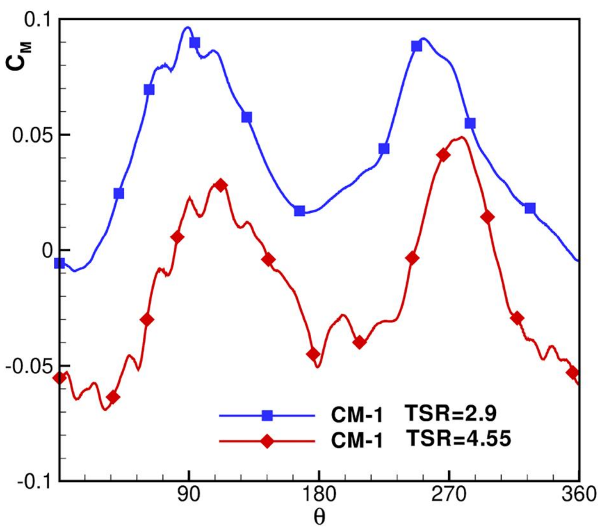

Fig. 8 Local torque coefficient at peak power and high-load: lower part of the rotor, slices −1

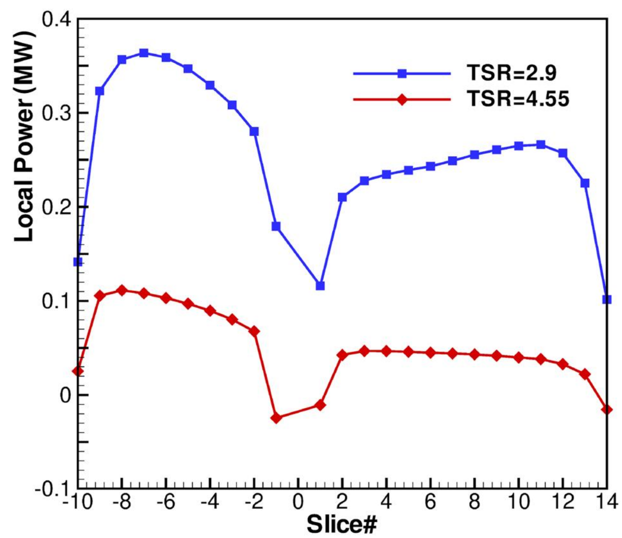

Fig. 10 Spanwise power harvesting: local performance evaluation at selected slices

At peak power condition, different behavior is taking place: less blockage is offered by the rotor, and in the upper part of the machine, as displayed for the spanwise position labeled Z_C^*, a reduced velocity deficit is found. Effective aerodynamic condition is indeed occurring in the upper half of the VAWT in virtue of more effective approaching freestream velocity.

To obtain a global description of the wake, the tracking of the minimum velocity defect region is considered spanwise. At each Z^*

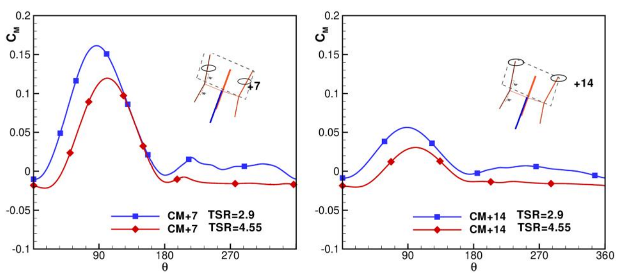

Fig. 9 Local torque coefficient at peak power and high-load: upper part of the rotor, slices +7, +14

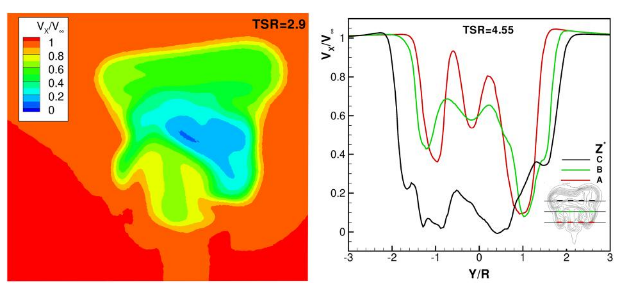

Fig. 11 Near wake at $X/D=2.0$, for TSR = 2.90: nondimensional streamwise velocity at varying spanwise positions Z^*

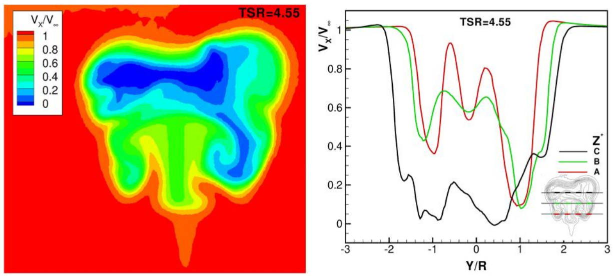

Fig. 12 Near wake at X/D=2.0, for TSR = 4.55: nondimensional streamwise velocity at varying spanwise positions Z^*

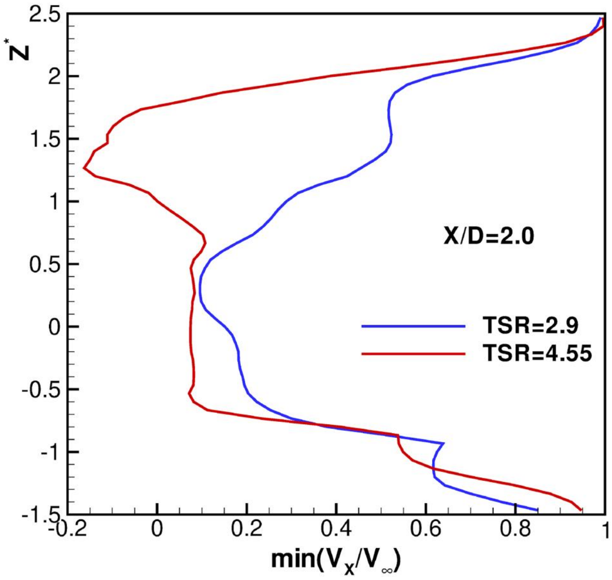

Fig. 13 Minimum velocity defect for TSR 2.9 and 4.55 at X/D=2.0

position, the minimum lateral velocity is reported in Fig. 13. These profiles highlight that the wake shape at peak power and the high load conditions differ to a greater extent in the upper part of the rotor. The aerodynamics affects most of the upwind revolution region; lower torque is gathered at high TSR, and major velocity defect takes place above the strut.

Finally, Fig. 14 presents a comparative view of the streamwise vortices shed from the blades at the two TSR values. It can be observed that these vortices are more pronounced under the high load case, owing to the increased viscous and blockage effects in this operation condition. Vortices are created from blades in previous revolutions and stem into perturbations traveling downstream. As clearly observed, the rotor shape determines in a direct way, the perturbation shape. Major blade–wake interaction occurs in the leeward region at high load. Probably due to its more accentuated vertical motions, the upper part becomes affected by more relevant transient perturbations. Instead, the high power condition is characterized by vortical structures affecting much smaller regions near to the blades or to the tip.

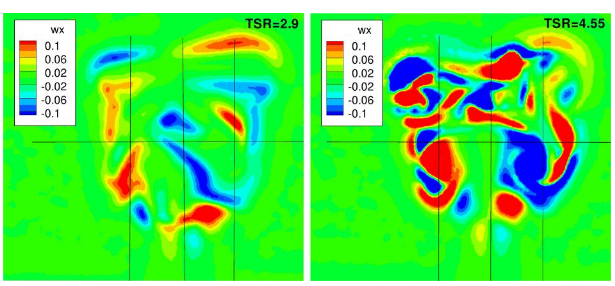

Fig. 14 Streamwise vorticity at TSR 2.9 and 4.55, cross section X/D=2.0

6 Concluding Remarks

In this work, we extended the aerodynamic analysis of an optimized design solution (HV2) aimed at improving performance under tilted operating conditions. Two relevant operating scenarios, namely, peak power and high load conditions, were studied. Given the offshore application focus, this study exclusively analyzed a large-scale model. The key findings from this investigation can be summarized as follows. From a global performance point of view, the machine is characterized by a peculiar behavior driven by the blade design coning angle

- The upper portion of the rotor from the holding strut, upward, features an aerodynamics in line with the one expected for an H-shaped VAWT.
- The lower portion of the rotor shows a modified torque with nearly the same profile in upwind and downwind.

Rapid velocity recovery can be promoted when a coning angle is adopted in virtue of vertical motion toward the tip. This effect is clearly also related to the operating condition; high drag may determine major viscous losses and increased vorticity in the near wake field. Therefore, the perturbation evolution need to be considered along with the general trend of the wake. These results provide valuable insights into the aerodynamic behavior of large-scale vertical-axis wind turbines in tilted conditions, supporting their feasibility for offshore applications and laying the groundwork for further future investigations. In fact as it is well known, the tilt angle effect is one of the relevant issues to consider in such installations. Better understanding of wind rotor aerodynamics can be useful to develop new blade designs considering both the local performance and the establishment of the wake itself. Offshore wind energy is ever more recognized as a key solution for the current energy transition, with wind turbines located far from the coast offering unique advantages. Research and knowledge on this perspective have thus a key role in the creation of a new green economy, sustainable, and affordable for the whole community.

Data Availability Statement

The datasets generated and supporting the findings of this article are obtainable from the corresponding author upon reasonable request.

Nomenclature

c = blade chord (m)
C_M = moment coefficient $C_M = M/(1/4\rho_\infty V_\infty^2 HD^2)$
C_P = power coefficient $C_P = C_M$TSR
D = turbine diameter (m)
H = turbine span (m)
L = turbine blade length (m)
M = moment (N·m)
N = number of blades
P = power (W)
R = turbine radius (m)
TSR = tip speed ratio
U = peripheral velocity (m/s)
V = absolute velocity (m/s)
VAWT = vertical-axis wind turbine
W = relative velocity (m/s)
X = streamwise coordinate (m)
Y = lateral coordinate (m)
Z = spanwise coordinate (m)
Z^* = nondimensional spanwise coordinate Z/L_{lower}

Greek Symbols

α = angle of attack
β = coning angle
θ = inclination/azimuthal angle

Appendix: Numerical Setup Validation

The numerical setup used in this work is based on former studies carried out by the authors, where dedicated validation against available measurement campaigns was given. The reliability and accuracy of the numerical settings have been herein assumed from a campaign pertaining to a similar wind turbine but at small lab scale. In Ref. [25], a thorough investigation on the performance of an H-shaped rotor, operating at design and off-design conditions, was presented both in terms of global and local flow features and parameters. In this section, the main results concerning the local aerodynamic performance and global near wake configuration are reported from cited works for the sake of completeness.

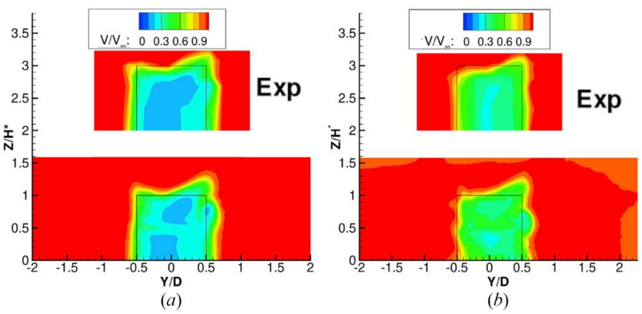

Fig. 15 Streamwise velocity field at near wake section $X/D = 0.75$ for experiments (top) and simulations (bottom). Design condition (*a*) TSR = 3.3 and off-design point (*b*) TSR = 2.4. Results already presented in Ref. [25].

Table 3 Power coefficient at two TSR values: numerics, experiments, and measurement uncertainty

TSR	Numerics	Experiments	Uncertainty
2.7	0.22	0.26	±0.015
3.3	0.25	0.28	±0.020

Results already presented in Ref. [25].

Taken from Ref. [25], Fig. 15 displays the near wake velocity field obtained by numerics against available experimental data. Good matching in between the two maps is observed at both operating conditions. Satisfactory accuracy of the computed flow field was also confirmed from a global perspective, as shown in Table 3 where the C_P values are listed for numerics and experiments. These results demonstrate a high reliability level of the adopted numerical setup, that can be assumed for similar small-scale wind rotors. For large-scale models, the same numerical configuration can be adopted in satisfactory manner, since MW rotors are characterized by a high Reynolds number regime. Indeed, as it is widely recognized, in this condition, the turbulence models are by far well established, and accurate results can therefore be expected.

References

[1] Zanforlin, S., and Nishino, T., 2016, "Fluid Dynamic Mechanisms of Enhanced Power Generation by Closely Spaced Vertical Axis Wind Turbines," Renewable Energy, **99**, pp. 1213–1226.
[2] Hezaveh, S. H., Bou-Zeid, E., Dabiri, J., Kinzel, M., Cortina, G., and Martinelli, L., 2018, "Increasing the Power Production of Vertical-Axis Wind-Turbine Farms Using Synergistic Clustering," Boundary-Layer Meteorol., **169**(2), pp. 275–296.
[3] Azadani, L., 2023, "Vertical Axis Wind Turbines in Cluster Configurations," Ocean Eng., **272**, p. 113855.
[4] Li, G., Xu, W., Li, Y., and Wang, F., 2022, "Univariate Analysis of Scaling Effects on the Aerodynamics of Vertical Axis Wind Turbines Based on High-Resolution Numerical Simulations: The Reynolds Number Effects," J. Wind Eng. Ind. Aerodyn., **223**, p. 104938.
[5] Kouaissah, O., Franchina, N., and Persico, G., 2024, "3D CFD Study of a DeepWind Demonstrator at Design, Off-Design and Tilted Operating Conditions," Energy, **291**, p. 130313.
[6] Kouaissah, O., Franchina, N., and Persico, G., 2025, "A Computational Fluid Dynamics Study on the Performance of Modified H-Shaped VAWTs for Tilted Operation Condition," ASME J. Eng. Gas Turbines Power, **147**(5), p. 051017.
[7] Hand, B., and Cashman, A., 2020, "A Review on the Historical Development of the Lift-Type Vertical Axis Wind Turbine: From Onshore to Offshore Floating Application," Sustainable Energy Technol. Assess., **38**, p. 100646.
[8] Ghigo, A., Faraggiana, E., Giorgi, G., Mattiazzo, G., and Bracco, G., 2024, "Floating Vertical Axis Wind Turbines for Offshore Applications Among Potentialities and Challenges: A Review," Renewable Sustainable Energy Rev., **193**, p. 114302.
[9] Orlando, A., Pagnini, L., and Repetto, M. P., 2021, "Structural Response and Fatigue Assessment of a Small Vertical Axis Wind Turbine Under Stationary and Non-Stationary Excitation," Renewable Energy, **170**, pp. 251–266.
[10] Liu, J., Lin, H., and Zhang, J., 2019, "Review on the Technical Perspectives and Commercial Viability of Vertical Axis Wind Turbines," Ocean Eng., **182**, pp. 608–626.
[11] Eboibi, O., Danao, L. A. M., and Howell, R. J., 2016, "Experimental Investigation of the Influence of Solidity on the Performance and Flow Field Aerodynamics of Vertical Axis Wind Turbines at Low Reynolds Numbers," Renewable Energy, **92**, pp. 474–483.
[12] Subramanian, A., Yogesh, S. A., Sivanandan, H., Giri, A., Vasudevan, M., Mugundhan, V., and Velamati, R. K., 2017, "Effect of Airfoil and Solidity on Performance of Small Scale Vertical Axis Wind Turbine Using Three Dimensional CFD Model," Energy, **133**, pp. 179–190.
[13] Wang, Y., Shen, S., Li, G., Huang, D., and Zheng, Z., 2018, "Investigation on Aerodynamic Performance of Vertical Axis Wind Turbine With Different Series Airfoil Shapes," Renewable Energy, **126**, pp. 801–818.
[14] Orlandi, A., Collu, M., Zanforlin, S., and Shires, A., 2015, "3D URANS Analysis of a Vertical Axis Wind Turbine in Skewed Flows," J. Wind Eng. Ind. Aerodyn., **147**, pp. 77–84.
[15] Scheurich, F., Fletcher, T., and Brown, R., 2010, "The Influence of Blade Curvature and Helical Blade Twist on the Performance of a Vertical-Axis Wind Turbine," 48th AIAA Aerospace Sciences Meeting Including the New Horizons Forum and Aerospace Exposition, Orlando, FL, Jan. 4–7.
[16] Leithead, W., Camciuc, A., Amiri, A. K., and Carroll, J., 2019, "The X-Rotor Offshore Wind Turbine Concept," IOP Conf. Ser.: J. Phys., **1356**(1), p. 012031.
[17] Flannigan, C., Carroll, J., and Leithead, W., 2022, "Operations Expenditure Modelling of the X-Rotor Offshore Wind Turbine Concept," IOP Conf. Ser.: J. Phys., **2265**(3), p. 032054.
[18] Mertens, S., van Kuik, G., and van Bussel, G., 2003, "Performance of an H-Darrieus in the Skewed Flow on a Roof," ASME J. Sol. Energy Eng., **125**(4), pp. 433–440.
[19] Senga, H., Umemoto, H., and Akimoto, H., 2022, "Verification of Tilt Effect on the Performance and Wake of a Vertical Axis Wind Turbine by Lifting Line Theory Simulation," Energies, **15**(19), p. 6939.
[20] Kouaissah, O., Franchina, N., Siddiqui, M., and Persico, G., 2024, "A Computational Study on the Performance and Wake Development of a Tilted H-Shaped VAWT Rotor," Renewable Energy, **222**, p. 119932.
[21] Chowdhury, A. M., Akimoto, H., and Hara, Y., 2016, "Comparative CFD Analysis of Vertical Axis Wind Turbine in Upright and Tilted Configuration," Renewable Energy, **85**, pp. 327–337.
[22] Rezaeiha, A., Kalkman, I., and Blocken, B., 2017, "CFD Simulation of a Vertical Axis Wind Turbine Operating at a Moderate Tip Speed Ratio: Guidelines for Minimum Domain Size and Azimuthal Increment," Renewable Energy, **107**, pp. 373–385.
[23] Franchina, N., Persico, G., and Savini, M., 2019, "2D-3D Computations of a Vertical Axis Wind Turbine Flow Field: Modeling Issues and Physical Interpretations," Renewable Energy, **136**, pp. 1170–1189.
[24] Menter, F. R., 1994, "Two-Equation Eddy-Viscosity Turbulence Model for Engineering Applications," AIAA J., **32**(8), pp. 1598–1605.
[25] Franchina, N., Persico, G., and Savini, M., 2020, "Three-Dimensional Unsteady Aerodynamics of a H-Shaped Vertical Axis Wind Turbine Over the Full Operating Range," J. Wind Eng. Ind. Aerodyn., **206**, p. 104273.
[26] Tescione, G., Ragni, D., He, C., Simão Ferreira, C. J., and van Bussel, G. J. W., 2014, "Near Wake Flow Analysis of a Vertical Axis Wind Turbine by Stereoscopic Particle Image Velocimetry," Renewable Energy, **70**, pp. 47–61.
[27] Wei, N. J., Brownstein, I. D., Cardona, J. L., Howland, M. F., and Dabiri, J. O., 2021, "Near-Wake Structure of Full-Scale Vertical-Axis Wind Turbines," J. Fluid Mech., **914**, pp. 1–40.
[28] Tjiu, W., Marnoto, T., Mat, S., Ruslan, M. H., and Sopian, K., 2015, "Darrieus Vertical Axis Wind Turbine for Power Generation II: Challenges in HAWT and the Opportunity of Multi-Megawatt Darrieus VAWT Development," Renewable Energy, **75**, pp. 560–571.
[29] Franchina, N., Kouaissah, O., Persico, G., and Savini, M., 2019, "Three-Dimensional CFD Simulation and Experimental Assessment of the Performance of a H-Shape Vertical-Axis Wind Turbine at Design and Off-Design Conditions," Int. J. Turbomach., Propul. Power, **4**(3), p. 30.